JACS
JOURNAL OF THE AMERICAN CHEMICAL SOCIETY
pubs.acs.org/JACS
Article

Is Deprotonation of the Oxygen-Evolving Complex of Photosystem II during the $S_1 \rightarrow S_2$ Transition Suppressed by Proton Quantum Delocalization?

Ke R. Yang, K. V. Lakshmi, Gary W. Brudvig, and Victor S. Batista*

Cite This: J. Am. Chem. Soc. 2021, 143, 8324−8332
Read Online
ACCESS | Metrics & More | Article Recommendations | Supporting Information

ABSTRACT: We address the protonation state of the water-derived ligands in the oxygen-evolving complex (OEC) of photosystem II (PSII), prepared in the S_2 state of the Kok cycle. We perform quantum mechanics/molecular mechanics calculations of isotropic proton hyperfine coupling constants, with direct comparisons to experimental data from two-dimensional hyperfine sublevel correlation (HYSCORE) spectroscopy and extended X-ray absorption fine structure (EXAFS). We find a low-barrier hydrogen bond with significant delocalization of the proton shared by the water-derived ligand, W1, and the aspartic acid residue D1−D61 of the D1 polypeptide. The lowering of the zero-point energy of a shared proton due to quantum delocalization precludes its release to the lumen during the $S_1 \rightarrow S_2$ transition. Retention of the proton facilitates the shuttling of a proton during the isomerization of the tetranuclear manganese−calcium−oxo (Mn_4Ca−oxo) cluster, from the "open" to "closed" conformation, a step suggested to be necessary for oxygen evolution from previous studies. Our findings suggest that quantum-delocalized protons, stabilized by low-barrier hydrogen bonds in model catalytic systems, can facilitate the accumulation of multiple oxidizing equivalents at low overpotentials.

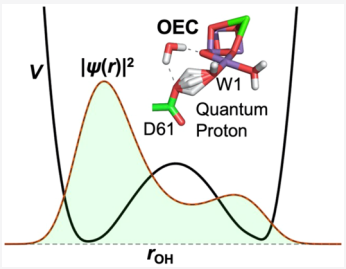

INTRODUCTION

Photosynthetic water oxidation involves the direct splitting of water into dioxygen, protons, and electrons using sunlight. The reaction is catalyzed by the oxygen-evolving complex (OEC) in the multisubunit membrane protein complex, photosystem II (PSII).[1−4] The OEC is composed of a tetranuclear manganese−calcium−oxo (Mn_4CaO_5) cluster in which the metal ions are linked by μ-oxo bridges. The water-oxidation reaction proceeds through the Kok cycle, which involves the transition of the OEC through four (semi)stable (S_0, S_1, S_2, and S_3) states and one unstable (S_4) state, where alternate steps involve the transfer of an electron or electron and proton. It is well established that the $S_0 \rightarrow S_1$, $S_1 \rightarrow S_2$, $S_2 \rightarrow S_3$, and $S_3 \rightarrow S_0$ transitions result in the release of 1, 0, 1, and 2 protons to the lumen, respectively[5,6] but the absolute protonation state of OEC in the S states remains unclear.[3,7,8] Knowledge of the protonation state is important as it determines the thermodynamic and catalytic reactivity of the OEC and is critical for a better understanding of the mechanism of light-driven water oxidation.

The position of heavy atoms in the dark-stable S_1 state of the OEC has been determined with increasing accuracy using novel high-resolution X-ray crystallography methods.[9−11] Recently, due to breakthroughs in X-ray free electron laser (XFEL) techniques, the structures of the S_2 and S_3 state have been resolved at nearly atomic resolution.[12−14] This has provided detailed structural information for computational analyses of the mechanism of the water-oxidation reaction. However, it is notable that protons are invisible in all of the X-ray crystal structures of PSII, which hinders the determination of the absolute protonation state of OEC and reliable computational modeling of the catalytic mechanism.

Among all of the S-state transitions of the OEC, the $S_1 \rightarrow S_2$ transition is the only one that does not involve the release of proton(s) to the lumen, which has allowed for the observation of the S_2 state at cryogenic temperatures.[15] The lack of proton release to the lumen during the $S_1 \rightarrow S_2$ transition may provide insight into the water-oxidation chemistry and has led to a suggestion that unique features observed in Fourier Transform infrared (FTIR) difference spectra of the OEC could be due to a protonated water cluster in the S_2 state.[16] The S_2 state has been extensively studied by continuous-wave and pulsed electron paramagnetic resonance (EPR),[17−25] extended X-ray absorption fine structure (EXAFS),[26−28] and FTIR difference spectroscopy.[16,29−32] There have been various suggestions on the possible protonation states of the S_2 state of which two representative types that involve the water-derived ligands, W1 and W2 (Figure 1), are noteworthy.[3] While W1 has always been assumed to be a water molecule that is directly hydrogen bonded to the carboxyl O atom of an aspartic acid residue in the D1 polypeptide, D1−D61, W2 was considered to be either

Received: January 18, 2021
Published: May 24, 2021

https://doi.org/10.1021/jacs.1c00633
J. Am. Chem. Soc. 2021, 143, 8324−8332

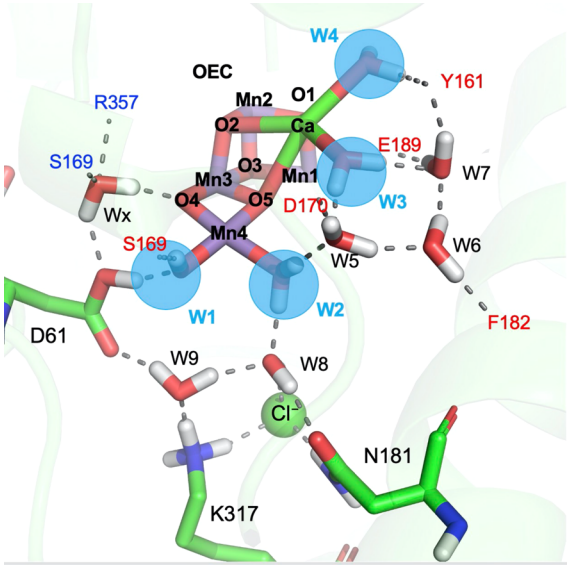

Figure 1. Water molecules, key amino acid residues, and Cl^- cofactor that are involved in the hydrogen-bonding network in the S_2 state of the OEC. The labels Mn1−M4, O1−O5, and Ca follow the standard notation. W1−W4 (highlighted in light blue) are water-derived ligands that are directly coordinated to the Mn and Ca ions in the OEC, W5−W9 are additional water molecules in the X-ray crystal structure[10] that form an extensive hydrogen-bonding network that is capped by amino-acid residues and a Cl^- ion, and W_x is a water molecule that is hydrogen bonded to the μ-oxo ligand, O4, in the OEC. The dashed lines in the model denote hydrogen bonds. The amino acid residues D61, N181, and K317 are explicitly shown in the model, while other residues capping the hydrogen-bonding network are represented by a one letter amino acid code followed by the residue number, where the blue and red fonts indicate hydrogen-bond donors and acceptors, respectively.

a water molecule (i.e., W2 = H_2O and O5 = μ-oxo)[33−35] or a hydroxide ligand (i.e., W2 = HO^- and O5 = μ-oxo).[36,37]

In this study, we investigate different models of the S_2 state of the OEC with varying protonation states of W1, W2, and D1−D61 in an extensive hydrogen-bonding network using quantum mechanical/molecular mechanical (QM/MM) methods (Figure 1). The resulting structural models are consistent with previously published EXAFS data[26] and two-dimensional (2D) hyperfine sublevel correlation (HYSCORE) spectroscopy.[23] In particular, we identify a proton in the S_2 state of the OEC that is highly quantum mechanical in nature as it is delocalized between the water-derived ligand, W1, and D1−D61. A comparison between the calculated hyperfine coupling constants (HFCs) of the shared proton model and the experimental couplings determined by 2D HYSCORE spectroscopy[23] provide direct evidence for quantum delocalization of the proton that is shared between W1 and D1−D61. These findings are in agreement with previous FTIR difference spectra[30] that displayed a feature at 2900/2740 cm^{-1} that can be attributed to transitions between different vibrational states of the quantum-delocalized proton. The presence of a quantum-delocalized proton in the S_2 state accounts for the absence of proton release in the $S_1 \rightarrow S_2$ transition. Moreover, it provides an explanation for the feasibility of the $S_1 \rightarrow S_2$ transition at cryogenic temperatures[15] and the presence of the open and closed conformers[36] of the catalytic Mn_4CaO_5 cluster in the S_2 state that are necessary for the $S_2 \rightarrow S_3$ transition during catalytic water oxidation.[38−40] Our results highlight the importance of quantum effects in the highly efficient water-oxidation reaction of PSII that powers the planet with solar energy.

RESULTS AND DISCUSSION

Recent X-ray crystal structures of the OEC[9−11] have revealed that the first-coordination shell of the Mn_4CaO_5 cluster is composed of Ca and Mn ions that are coordinated by μ-oxo (O^{2-}) bridges, amino acid side chains, and four terminal water-derived ligands, namely, W1 and W2 at the Mn4 ion and W3 and W4 at the Ca ion (Figure 1). However, the second coordination shell as well as shells that are farther away are less defined in these structures. Pokhrel and Brudvig[41] have highlighted the importance of the hydrogen-bonding network that encompasses D1−D61 and water-derived ligands in the OEC by correlating the X-ray crystal structures with data from EPR spectroscopy. The XFEL crystal structures have indicated that the position of some of the water molecules in the OEC remain unchanged during the S-state transitions.[12,14] In order to better understand the changes upon S-state transitions of the OEC, we expanded the QM region of our previous QM/MM model of the S_2 state[42] to include an extensive hydrogen-bonding network involving more water molecules and amino acid residues surrounding the OEC. We find that by increasing the number of water molecules in the QM region, the hydrogen-bonding network now extends all the way from the Mn_4CaO_5 cluster to the backbone or side-chain atoms of the amino acid residues and Cl^- cofactor of the OEC (Figure 1).

The inclusion of an extensive network of hydrogen bonds in our model provides a more realistic description of the hydrogen-bonding interactions in the OEC; it is also helpful as it places physical constraints on the specific pattern of hydrogen bonds. For example, when the water molecule, W6, and the backbone carbonyl O atom of D1-F182 (denoted as O-D1-F182) are within hydrogen-bonding distance, W6 acts as a hydrogen-bond donor to D1-F182 since O-D1-F182 can only serve as an acceptor. As a result, W6 serves as a hydrogen-bond acceptor to W5, which in turn accepts a proton from W2. Thus, if the D1-F182 residue was not included in the model, as was the case in most of the previous theoretical studies,[36,37] the hydrogen-bonding interaction between W5 and O-D1-F182 would be absent. Instead, the model would contain alternate hydrogen-bonding partners whereby W6 would either serve as a hydrogen-bond acceptor or donor to W5 which in turn would serve as either a hydrogen-bond acceptor or donor to W2. In order to avoid this discrepancy, we considered an extensive network of hydrogen bonds (Figure 1) to obtain a more accurate description of the hydrogen-bonding interactions in the OEC (see section S2 for details).

In conjunction with the extensive hydrogen-bonding network described above, we considered various protonation states of the water-derived ligands and the D1−D61 residue in the S_2 state of the OEC: (**A**) protonated D1−D61 side chain with W1 and W2 as OH^- and H_2O ligands, respectively, (**B**) deprotonated D1−D61 with both W1 and W2 as H_2O ligands, and (**C**) protonated D1−D61 with W1 and W2 as H_2O and OH^- ligands, respectively. We optimized the structure of each of the possible states by carefully adjusting the hydrogen-bonding interactions in the OEC (Figure 2, structures **A**−**C**).

The core structure of the Mn_4CaO_5 cluster in the OEC is similar for the three protonation-state models (Figure 2, structures **A**−**C**). The identical number of atoms in each structure allows for a comparison of the relative energies. We

https://doi.org/10.1021/jacs.1c00633
J. Am. Chem. Soc. 2021, 143, 8324−8332

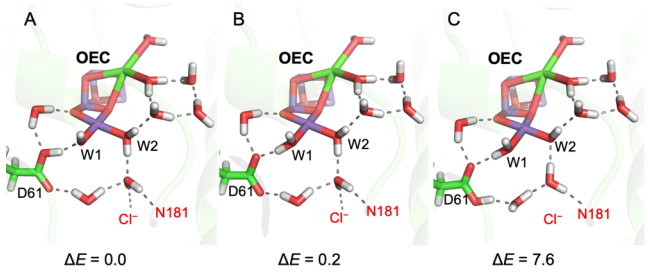

Figure 2. Optimized QM/MM structures of the S_2 state with different protonation states of W1, W2, and D1−D61 residues and their relative energies in kcal/mol (using the energy of structure **A** as a reference): (**A**) W1, OH^-; W2, OH_2; and D1−D61, COOH; (**B**) W1, OH_2; W2, OH_2; and D1−D61, COO^-; (**C**) W1, OH_2; W2, OH^-; and D1−D61, COOH.

observe that structure **A** with a protonated D1−D61 residue, W1 as OH^- and W2 as H_2O in Figure 2A has the lowest relative energy suggesting that it is more likely to represent the protonation state in the S_2 state of the OEC. The relative energy of structure **B** is only slightly higher; however, the energy of structure **C** (protonated D1−D61, W1 as H_2O and W2 as OH^-) is 7.6 kcal/mol higher than that of structure **A** (Figure 2). This is due to the loss of a hydrogen bond as W_2 is an OH^- ligand that acts as a hydrogen-bond acceptor.

Structure **B** has previously been suggested to be consistent with experimental EXAFS results.[42] EXAFS has been successfully employed to elucidate the structural changes due to change in the oxidation state or topology of the metal ions,[26−28] e.g., the open and closed conformers of the Mn_4CaO_5 cluster in the S_2 state of the OEC. Thus, it can be used to identify unreasonable (or infeasible) structures and serve as a stringent test for the structural models in this study. We simulated the EXAFS spectra for the structures **A**−**C** with varying protonation states of the water-derived ligands and D1−D61 residue (Figure S2). As evident in Figure S2, the simulated EXAFS spectra of structures **A**−**C** with different protonation patterns are similar, which is expected due to the similarity of the Mn_4CaO_5 core in each structure. More importantly, the simulated spectra in Figure S2 reproduce the experimental EXAFS spectra in both the *k*- and reduced-distance space. Thus, it is not possible to distinguish between the different protonation states of the S_2 state of the OEC using EXAFS. However, based on the QM/MM energetics in the present study, the protonation states in structures **A** and **B** are more likely than structure **C** in the S_2 state.

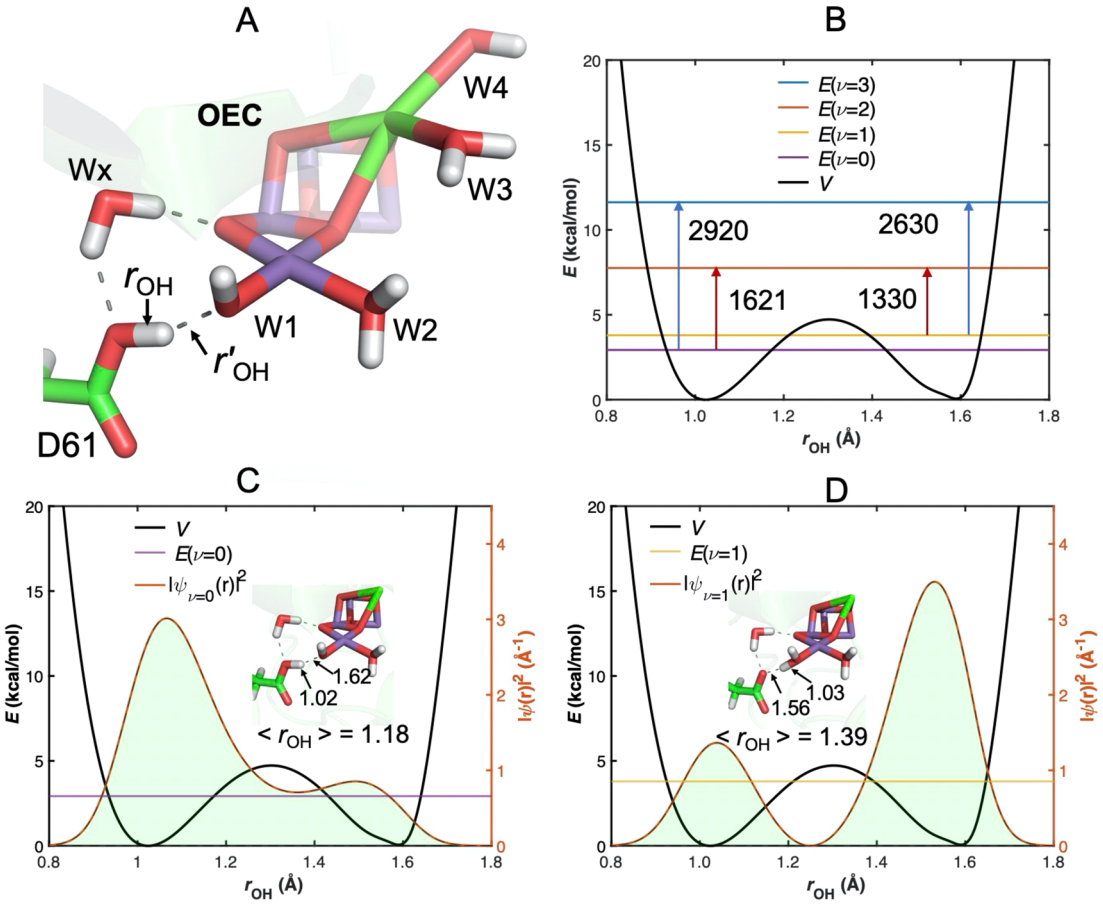

Figure 3. Quantum-delocalized proton between W1 and D1−D61 in the S_2 state of the OEC. (A) Structure of D1−D61 and water molecules in the OEC with r_{OH} and r'_{OH} denoting distances between the quantum proton and O atoms in D1−D61 and W1, respectively. (B) Potential energy curve along r_{OH}. The energy eigenvalues of the four lowest vibrational states and excitation energies between different vibrational states are in cm^{-1}; Probability density $|\psi(r)|^2$ of the ground (C) and first excited (D) vibrational states. The expectation values of r_{OH} are in angstroms. The inset structures in C and D correspond to the classical structures under the Born−Oppenheimer approximation with the proton located at D1−D61 and W1, respectively. The expectation values of r_{OH}, evaluated from quantum mechanical vibrational wave functions, deviate significantly from the r_{OH} in the classical structures, indicating the strong quantum delocalized nature of the proton that is shared between W1 and D1−D61.

https://doi.org/10.1021/jacs.1c00633
J. Am. Chem. Soc. 2021, 143, 8324−8332

Among all of the S-state transitions, the $S_1 \rightarrow S_2$ transition is the only one that does not release a proton to the lumen. Previously, FTIR difference spectroscopy measurements by Polander and Barry[16] revealed a broad IR band at 2880 cm^{-1}, and a more recent study revealed several unique features at ~2740 and 2900 cm^{-1} in the $S_1 \rightarrow S_2$ transition.[30] This led to proposals for the presence of a protonated water cluster in the S_2 state.[16,30,43] However, to date, there is a lack of structural evidence for a protonated water cluster in the S_2 state of the OEC. Moreover, water is a poor base and is unlikely to be protonated in the presence of more easily protonatable groups, such as, carboxylate groups. Therefore, we investigated whether the FTIR data could be accounted for by structures **A**–**C** in Figure 2.

The similar energetics of structure **A** and **B** with differing protonation patterns leads to an obvious question as to which of the two structures best describes the protonation state of the S_2 state. We investigated the potential energy curves of a model with a proton located between W1 and the carboxyl O atom in D1–D61 (Figure 3A) by translating the shared proton between W1 and D1–D61. The potential energy curve along the O–H reaction coordinate is obtained by relaxed potential energy surface scan by fixing the two O–H bond lengths while optimizing the other degree of freedom. The potential energy as a function of r_{OH} is shown in Figure 3B (r_{OH} and r'_{OH} are defined in Figure 3A). As expected, there are two minima along the potential energy curve that correspond to the protonation pattern **A** (r_{OH} = 1.02 Å and r'_{OH} = 1.62 Å) and the protonation pattern **B** (r_{OH} = 1.56 Å and r'_{OH} = 1.03 Å). We observe that the potential energy near the two minima is highly anharmonic and the potential energy curve is best described as a "double-well potential". This is similar to a recent study by Kawashima et al.,[44] who suggested a strong interaction between W1 and D1–D61. As expected, the harmonic-approximation treatment of the motion of this proton is inadequate. When we solve the Schrödinger equation of this proton quantum mechanically, we find the ground (ν = 0) and first excited (ν = 1) vibrational states are close in energy (Figure 3B).

On the Born–Oppenheimer potential energy surface (BO PES), the protonation pattern of structure **A** with the proton bonded to the carboxyl O atom has r_{OH} = 1.02 Å and r'_{OH} = 1.62 Å, while the protonation pattern of structure **B** with the proton bonded to W1 has r_{OH} = 1.56 Å and r_{OH} = 1.03 Å. The ground vibrational state (ν = 0) has a large probability density between the O atoms of D61 and W1. Using the probability density of the ν = 0 state (Figure 3C), we calculated the expectation value of r_{OH} to be 1.18 Å, which deviates significantly from r_{OH} = 1.02 Å in the classical structure on the BO PES. The first excited vibrational state (ν = 1) has a large probability density at the two potential energy minima (Figure 3D), but it is also delocalized over a wide range. The expectation value of r_{OH} = 1.39 Å also deviates significantly from r_{OH} = 1.55 Å in the classical structure of the protonation pattern in structure **B** on the BO PES. In this respect, the protonation patterns of structures **A** and **B** can be regarded as the classical picture of the ground and first vibrational excitation state, respectively, of the delocalized proton between W1 and D1–D61 in the S_2 state. However, as the probability density suggests the proton is highly quantum mechanical in nature and is delocalized between the O atoms of W1 and D1–D61. Such delocalized protons have previously been observed in the enzyme, ketosteroid isomerase, in the presence of strong hydrogen-bonding interactions.[45]

Given the unique nature of the proton between W1 and D1–D61, we also considered other higher vibrational excitation states to facilitate comparison with previous FTIR difference spectroscopy studies.[16,29−31] We observed that the excitation from ν = 0 to ν = 2 and ν = 3 required energies of 1621 and 2920 cm^{-1}, while the excitation from ν = 1 to ν = 2 and ν = 3 required energies of 1330 and 2630 cm^{-1} (Figure 3B). Interestingly, the excitation energies from the ν = 0 and ν = 1 to ν = 3 vibrational states are consistent with the unique features at ~2900 and 2740 cm^{-1} that were observed in previous FTIR difference spectra.[30] Furthermore, there are spectral features in the 1700–1150 cm^{-1} region in the S_2-minus-S_1 FTIR difference spectra that were not previously assigned.[29] According to our simulations, some of these features arise from excitations from ν = 0 and ν = 1 to ν = 2 vibrational states. Thus, although the FTIR features were previously suggested to arise from a protonated water cluster, they are more consistent with the presence of a quantum-delocalized proton between W1 and D1–D61 at the S_2 state. Indeed, a site-directed mutagenesis study by Debus suggests that the presence of the D1–D61 residue correlates with the broad feature in the 2800 cm^{-1} region.[31]

Although the QM/MM energetics in our study suggests that structure **A** with the D1–D61 residue protonated and W1 and W2 as OH^- and H_2O ligands is the lowest in energy and the simulated EXAFS spectra for structure **A** are consistent with the experimental spectra of the S_2 state, direct evidence is needed to unambiguously establish the protonation state of the water-derived ligands in the S_2 state. Proton hyperfine coupling constants provide direct insight on the magnetic interaction between nuclear spin (I = 1/2) of protons and the unpaired electron spin (S = 1/2) in the S_2 state and are sensitive to the protonation state of OEC. One of us has previously performed two-dimensional (2D) hyperfine sublevel correlation (HYSCORE) spectroscopic studies of the proton hyperfine interactions in the S_2 state of the OEC in which we identified five groups of hyperfine-coupled protons, H^I–H^V.[23] On the basis of comparisons with di-μ-oxo dimanganese models[46,47] and the active site of superoxidized manganese catalase,[48] H^I and H^{III} were tentatively assigned to protons of the water-derived ligands, W1 and W2, H^{II} to the side chain of the D1-H332 residue, H^{IV} to hydrogen-bonded water molecules, and H^V to remote matrix protons in the vicinity of the Mn_4CaO_5 cluster in the OEC.

We validate the DFT methods by calculating the hyperfine coupling constants for the protons of mixed-valence di-μ-oxo dimanganese models where the calculated and experimental hyperfine couplings are in good agreement (Table S1).[46] We calculated the hyperfine coupling constants of protons in the protonation-state structures **A** and **B** of the S_2 state (Table S6). Our calculations indicate that the isotropic hyperfine coupling constant, A_{iso}, for an OH^- ligand coordinated to a Mn(IV) ion, is ~5–7 MHz, whereas the A_{iso} for an H_2O molecule coordinated to a Mn(IV) ion is 1–2 MHz. Given the similar energy of structure **A** and **B** and the quantum-delocalized nature of the proton between D1–D61 and W1, we take the average of the calculated proton hyperfine coupling constants over protonation-state structures **A** and **B** (Table 1). We obtain five groups of hyperfine-coupled protons, which is consistent with previous EPR experiments.[23] A comparison of the calculated and experimental isotropic hyperfine coupling

https://doi.org/10.1021/jacs.1c00633
J. Am. Chem. Soc. 2021, 143, 8324–8332

Table 1. Calculated Isotropic Proton Hyperfine Coupling Constants (HFCs) of the S_2 State Averaged over Structure A and B[a]

hydrogen atoms	A_{iso} (MHz) calcd structure **A** + **B**	A_{iso} (MHz) expt	assignment
H(W2)	1.5	±1.8 (±0.4)	H^{I}
H_{E1}(H332)	−0.7	±0.1 (±0.4)	H^{II}
H(W1)	3.0	±2.6 (±0.2)	H^{III}
H_{E2}(H337)	0.1	±0.2 (±0.2)	H^{IV}
$H(W_x)$	−0.2	±0.4 (±0.6)	H^{V}

[a]Also shown are the experimental hyperfine coupling constants that were previously measured by 2D HYSCORE spectroscopy and their tentative assignments.[23]

constants of the OEC suggests that H^{I} is best assigned a water ligand at a Mn(IV) ion which is most likely W2 at the Mn4 ion with an oxidation state of +IV and H^{II} is the proton(s) of an amino acid ligand coordinated at the Mn(III) ion which is the H_{E1} atom of D1-H332 at the Mn1 ion with an oxidation state of +III. Most interestingly, the A_{iso} value of the H^{III} group of protons (±2.6 MHz) that was previously assigned to a water ligand is larger than the A_{iso} of the water ligand at the Mn4 ion (1.3, 1.7, and 1.8 MHz) but smaller than the A_{iso} of OH^{-} (4.2 MHz) (Table S6). This is consistent with the presence of a quantum-delocalized proton where W1 is a combination of the classical water and OH^{-} ligand. Indeed, taking average of the calculated proton hyperfine coupling constants of the **A** and **B** structures yields an A_{iso} of W1 that is in agreement with the experimentally measured A_{iso} value for H^{III} (Table 1). Thus, the proton hyperfine coupling constant of W1 that was observed experimentally is consistent with a combination of classical H_2O and OH^{-} ligands, which is exactly what is expected for a quantum-delocalized proton between W1 and D1−D61. The A_{iso} value of protons in W1 from the quantum-delocalized proton model in our study is consistent with a previous report in literature where the calculated A_{iso} value for the proton of an OH^{-} ligand coordinated to the Mn4 ion in the S_2 state was 3.0 MHz.[49] However, at the time, the OH^{-} ligand in the experimental study was assigned as W_2 instead of W_1 (ref 23).

We are curious as to why nature would employ a quantum-delocalized proton in the S_2 state of the OEC. It is a well-known fact that delocalization of electrons greatly lowers the energy, as is the case with aromatic compounds. A proton, while 1836 times heavier than an electron is still lighter than other nuclei and is thus expected to have some quantum mechanical character. In structure **A**, the harmonic vibration frequency of the O−H stretch of the classical proton between D1−D61 and W_1 is ∼2700 cm^{-1} (Figure S7), corresponding to a zero-point energy of 3.9 kcal/mol, which is already decreased from the smaller than typical O−H stretching frequency in H_2O or a carboxyl group of ∼3000 cm^{-1} due to the strong hydrogen-bond interaction between W1 and the carboxyl group in D1−D61. The vibrational frequency of the shared proton is further decreased to ∼2000 cm^{-1} due to quantum delocalization along the O−H coordinate, corresponding to a lower zero-point energy of only 2.9 kcal/mol. Thus, the energy of the proton decreases through delocalization similar to that of electrons. It has been suggested that there is a strong hydrogen-bonding interaction between the D1-Y161 (Y_Z) residue and its conjugate hydrogen-bond acceptor, D1-H190.[50,51] The strong hydrogen-bonding interaction between Y_Z and D1-H190 that has been characterized as a low-barrier hydrogen bond with a delocalized proton between Y_Z and D1-H190 not only facilitates the oxidation of Y_Z by the primary donor cation, P_{680}^{+}, but also retains the oxidation power to oxidize the Mn_4CaO_5 cluster. In the $S_1 \rightarrow S_2$ transition, an electron is transferred from Mn4 to the $Y_Z^{\bullet}$−D1-H190 pair, accompanied by the formation of a quantum-delocalized proton between W_1 and D1−D61. The formation of a quantum delocalized proton promotes efficient electron transfer from the Mn_4CaO_5 cluster to the $Y_Z^{\bullet}$−D1-H190 pair (Scheme 1). When an electron is transferred from the Mn4 ion

Scheme 1. Schematic Representation of Electron Transfer from the $S_1Y_Z^{\bullet}$ to the S_2Y_Z State through the Formation of Two Low-Barrier Hydrogen Bonds

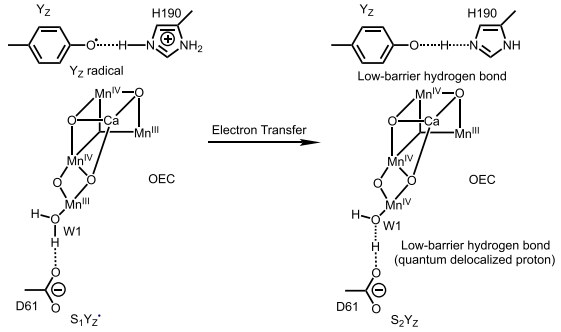

to $Y_Z^{\bullet}$, the pK_a of the water molecule W1 which is coordinated to an Mn(IV) ion decreases significantly to match the pK_a of D1−D61, resulting in a strong hydrogen-bonding interaction between W1 and D1−D61 and a quantum-delocalized proton between them. We are aware that proton transfer from W1 to D1−D61 has been observed in a previous QM/MM molecular dynamics simulation in the $S_2 \rightarrow S_3$ transition.[39] Therefore, we propose that in the $S_1 \rightarrow S_2$ transition there is a quantum-delocalized proton between W1 and D1−D61, which facilitates electron transfer from Mn4 to $Y_Z^{\bullet}$. The presence of a quantum-delocalized proton is consistent with the lack of deprotonation to the lumen that has been observed in the $S_1 \rightarrow S_2$ transition.

Extensive experimental studies have shown that there is no proton release to the lumen during the $S_1 \rightarrow S_2$ transition,[5,6,52,53] consistent with earlier theoretical studies.[42,54−56] In fact, experiments show that deprotonation occurs only after Y_Z gets oxidized to $Y_Z^{\bullet}$ during the $S_2 \rightarrow S_3$ transition.[5,6,52,53] However, the protonation state of the OEC in the S_2 state has remained uncertain. Here, we characterize the protonation state of the OEC supported by calculations of proton hyperfine coupling constants and direct comparison with HYSCORE measurements. We find that the S_2 state involves proton delocalization between D1−D61 and W1. The delocalized proton eigenstates obtained with rigorous quantum mechanical calculations are consistent with FTIR measurements.

It is interesting that the S_2 state displays two spin isomers with low-spin g = 2.0 and high-spin g = 4.1 EPR signals that have been attributed to the open and closed conformers of the Mn_4CaO_5 cluster in the OEC.[36] The low-spin g = 2.0 isomer is the stable form under normal buffer conditions, while the high-spin g = 4.1 isomer has been suggested to play a role in the $S_2 \rightarrow S_3$ transition.[25,38−40,57−59] In the low-spin open conformer of the S_2 state, the Mn1 ion is in a +III oxidation state, while the Mn4 ion is in a +IV oxidation state. However, in the high-

https://doi.org/10.1021/jacs.1c00633
J. Am. Chem. Soc. 2021, 143, 8324−8332

spin closed conformer of the S_2 state, the Mn1 ion is in a +IV oxidation state while Mn4 is in a +III oxidation state.[36] Previous studies on Mn model complexes have shown that H_2O ligands coordinated to a Mn(III) ion have higher pK_as and thus prefer to remain as neutral water molecules, while there is a decrease in the pK_a of H_2O ligands coordinated to a Mn(IV) ion which results in either a H_2O or OH^- ligand depending on the surrounding environment.[60] Therefore, one would expect that the protonation state of the water ligands in the low-spin open and high-spin closed conformer are different.

As shown in Figure 4, during the isomerization of the low-spin g = 2.0 open conformer to the high-spin g = 4.1 closed

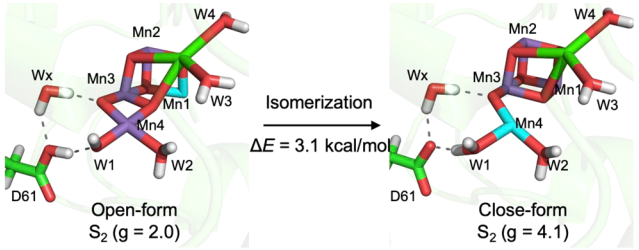

Figure 4. Shuttling of a proton during the isomerization between the open form (g = 2.0) and closed form (g = 4.1) of the S_2 states and the associated oxidation state and protonation state changes. Purple and cyan denote Mn(IV) and Mn(III) centers, respectively.

conformer, an electron is transferred from Mn1 to Mn4 ion and the proton between W1 and D1−D61 moves back to W1 to have a H_2O ligand when the Mn4 ion is in a +III oxidation state. In other words, the g = 2.0 and g = 4.1 isomerization of the S_2 state is accompanied by the movement of a proton between W1 and D1−D61. This is consistent with a previous study that demonstrated that an H/D kinetic isotope effect of 2.5 is associated with the spin-state isomerization.[57] It is of interest to note that a previous classical multiconformer continuum electrostatics (MCCE) study of the S_2 state also suggests that a water-derived ligand tends to be partially deprotonated in the g = 2.0 open conformer and be neutral in the g = 4.1 close conformer; although the partially deprotonnated water-derived ligand is suggested to be W2.[56] Our calculations indicate a slight energy preference for the g = 2.0 open conformer; however, the energy preference could be switched as the S-states proceed. Mn(III) ions tend to be pentacoordinated or hexacoordinated with a long Jahn−Teller axis and the orientation of the Jahn−Teller axis can greatly affect the geometric and electronic structure of Mn complexes. A recent study by Pantazis and co-workers[61] has shown the reorientation of the Jahn−Teller axis at Mn4 results in isomerism in the dark-stable S_1 state and is attributed to be the electronic origin of the valence isomerism in the S_2 state. Only one Mn(III) center is present in the S_2 state, the Jahn−Teller axis is oriented along the O5 and E189 at Mn1 in the open-form and oriented along W1 and O5 at Mn4 in the closed-form. The lowering of the oxidation state of Mn4 and the increase of the Mn−O distance between Mn4 and W1 along the Jahn−Teller axis lower the pK_a of W1 in the g = 4.1 closed conformer, favoring a neutral water ligand for W1. We have not had any success in locating other redox isomers with Mn2 or Mn3 in oxidation state III, probably due to the requirement of a Jahn−Teller distortion to stabilize Mn(III). The presence of a quantum-delocalized proton between W1 and D1−D61 facilitates the isomerization of the open and closed forms of the S_2 state through the shuttling of a proton, which will have important mechanistic consequences for S-state advancement in the catalytic water-oxidation reaction if the high-spin g = 4.1 isomer plays a role in the $S_2 \rightarrow S_3$ transition as suggested by previous studies.[25,38−40,57−59,62]

CONCLUSION

In summary, we have studied the protonation state of the S_2 state in the presence of an extensive hydrogen-bonding network in and around the OEC. Based on QM/MM calculations and explicit quantum mechanical treatment of the proton between W1 and D1−D61, we identify a quantum-delocalized proton between W1 and D1−D61 in the S_2 state. The presence of a quantum-delocalized proton is consistent with experimental EXAFS, difference FTIR, and 2D HYSCORE spectroscopy measurements. Quantum delocalization decreases the zero-point energy of the proton between W1 and D1−D61, which may account for the long-standing mystery that proton release to the lumen is absent during the $S_1 \rightarrow S_2$ transition. Proton delocalization is expected to facilitate electron transfer from the Mn_4CaO_5 cluster to $Y_Z^{\bullet}$ and enable a proton shuttling during the spin isomerization of the S_2 state from the open to the closed conformation. We anticipate that tuning the relative pK_a of the water ligands of biomimetic synthetic catalysts with proton-accepting groups that establish low-barrier hydrogen bonds may lead to the realization of quantum-delocalized protons that facilitate the accumulation of oxidizing equivalents under low overpotentials.

ASSOCIATED CONTENT

Supporting Information

The Supporting Information is available free of charge at https://pubs.acs.org/doi/10.1021/jacs.1c00633.

Computational details, structures of the S_2 state model in different protonation states (PDF)

Optimized structure A (PDB)

Optimized structure C (PDB)

Optimized structure B (PDB)

AUTHOR INFORMATION

Corresponding Author

Victor S. Batista − *Department of Chemistry, Yale University, New Haven, Connecticut 06520-8107, United States;* orcid.org/0000-0002-3262-1237; Email: victor.batista@yale.edu

Authors

Ke R. Yang − *Department of Chemistry, Yale University, New Haven, Connecticut 06520-8107, United States;* orcid.org/0000-0003-0028-2717

K. V. Lakshmi − *Department of Chemistry and Chemical Biology and The Baruch '60 Center for Biochemical Solar Energy, Rensselaer Polytechnic Institute, Troy, New York 12180, United States;* orcid.org/0000-0001-5443-9017

Gary W. Brudvig − *Department of Chemistry, Yale University, New Haven, Connecticut 06520-8107, United States;* orcid.org/0000-0002-7040-1892

Complete contact information is available at: https://pubs.acs.org/10.1021/jacs.1c00633

Author Contributions

The manuscript was written by K.R.Y. with contributions from all authors. The research was supervised by V.S.B. All authors have given approval to the final version of the manuscript.

Notes

The authors declare no competing financial interest.

■ ACKNOWLEDGMENTS

The authors acknowledge support from the Photosynthetic Systems Program, Office of Basic Energy Sciences, United States Department of Energy, under Contract Nos. DESC0001423 (V.S.B.), DE-FG02-05ER15646 (G.W.B.), and DE-FG02-07ER15903 (K.V.L.). We thank the National Energy Research Scientific Computing Center (NERSC) and Yale Center for Research Computing (YCRC) for computing time.

■ ABBREVIATIONS

BO PES, Born−Oppenheimer potential energy surface; EPR, electron paramagnetic resonance; EXAFS, extended X-ray absorption fine structure; FTIR, Fourier transform infrared; HFC, hyperfine coupling constant; HYSCORE, hyperfine sublevel correlation; OEC, oxygen-evolving complex; PSII, photosystem II; QM/MM, combined quantum mechanics/molecular mechanics; XFEL, X-ray free electron laser

■ REFERENCES

(1) McEvoy, J. P.; Brudvig, G. W. Water-splitting chemistry of photosystem II. *Chem. Rev.* **2006**, *106*, 4455−4483.
(2) Yano, J.; Yachandra, V. Mn4Ca cluster in photosynthesis: Where and how water is oxidized to dioxygen. *Chem. Rev.* **2014**, *114*, 4175−4205.
(3) Askerka, M.; Brudvig, G. W.; Batista, V. S. The O_2-evolving complex of photosystem II: Recent insights from quantum mechanics/molecular mechanics (QM/MM), extended X-ray absorption fine structure (EXAFS), and femtosecond X-ray crystallography data. *Acc. Chem. Res.* **2017**, *50*, 41−48.
(4) Vinyard, D. J.; Brudvig, G. W. Progress toward a molecular mechanism of water oxidation in photosystem II. *Annu. Rev. Phys. Chem.* **2017**, *68*, 101−116.
(5) Zaharieva, I.; Wichmann, J. M.; Dau, H. Thermodynamic limitations of photosynthetic water oxidation at high proton concentrations. *J. Biol. Chem.* **2011**, *286*, 18222−18228.
(6) Klauss, A.; Haumann, M.; Dau, H. Alternating electron and proton transfer steps in photosynthetic water oxidation. *Proc. Natl. Acad. Sci. U. S. A.* **2012**, *109*, 16035−16040.
(7) Chen, H.; Case, D. A.; Dismukes, G. C. Reconciling Structural and Spectroscopic Fingerprints of the Oxygen-Evolving Complex of Photosystem II: A Computational Study of the S_2 State. *J. Phys. Chem. B* **2018**, *122*, 11868−11882.
(8) Chen, H.; Dismukes, G. C.; Case, D. A. Resolving Ambiguous Protonation and Oxidation States in the Oxygen Evolving Complex of Photosystem II. *J. Phys. Chem. B* **2018**, *122*, 8654−8664.
(9) Tanaka, A.; Fukushima, Y.; Kamiya, N. Two different structures of the oxygen-evolving complex in the same polypeptide frameworks of photosystem II. *J. Am. Chem. Soc.* **2017**, *139*, 1718−1721.
(10) Umena, Y.; Kawakami, K.; Shen, J.-R.; Kamiya, N. Crystal structure of oxygen-evolving photosystem II at a resolution of 1.9 Å. *Nature* **2011**, *473*, 55−60.
(11) Suga, M.; Akita, F.; Hirata, K.; Ueno, G.; Murakami, H.; Nakajima, Y.; Shimizu, T.; Yamashita, K.; Yamamoto, M.; Ago, H.; Shen, J.-R. Native structure of photosystem II at 1.95 Å resolution viewed by femtosecond X-ray pulses. *Nature* **2015**, *517*, 99−103.
(12) Kern, J.; Chatterjee, R.; Young, I. D.; Fuller, F. D.; Lassalle, L.; Ibrahim, M.; Gul, S.; Fransson, T.; Brewster, A. S.; Alonso-Mori, R.; Hussein, R.; Zhang, M.; Douthit, L.; de Lichtenberg, C.; Cheah, M. H.; Shevela, D.; Wersig, J.; Seuffert, I.; Sokaras, D.; Pastor, E.; Weninger, C.; Kroll, T.; Sierra, R. G.; Aller, P.; Butryn, A.; Orville, A. M.; Liang, M.; Batyuk, A.; Koglin, J. E.; Carbajo, S.; Boutet, S.; Moriarty, N. W.; Holton, J. M.; Dobbek, H.; Adams, P. D.; Bergmann, U.; Sauter, N. K.; Zouni, A.; Messinger, J.; Yano, J.; Yachandra, V. K. Structures of the intermediates of Kok's photosynthetic water oxidation clock. *Nature* **2018**, *563*, 421−425.
(13) Suga, M.; Akita, F.; Yamashita, K.; Nakajima, Y.; Ueno, G.; Li, H.; Yamane, T.; Hirata, K.; Umena, Y.; Yonekura, S.; Yu, L.-J.; Murakami, H.; Nomura, T.; Kimura, T.; Kubo, M.; Baba, S.; Kumasaka, T.; Tono, K.; Yabashi, M.; Isobe, H.; Yamaguchi, K.; Yamamoto, M.; Ago, H.; Shen, J.-R. An oxyl/oxo mechanism for oxygen-oxygen coupling in PSII revealed by an x-ray free-electron laser. *Science* **2019**, *366*, 334−338.
(14) Ibrahim, M.; Fransson, T.; Chatterjee, R.; Cheah, M. H.; Hussein, R.; Lassalle, L.; Sutherlin, K. D.; Young, I. D.; Fuller, F. D.; Gul, S.; Kim, I.-S.; Simon, P. S.; de Lichtenberg, C.; Chernev, P.; Bogacz, I.; Pham, C. C.; Orville, A. M.; Saichek, N.; Northen, T.; Batyuk, A.; Carbajo, S.; Alonso-Mori, R.; Tono, K.; Owada, S.; Bhowmick, A.; Bolotovsky, R.; Mendez, D.; Moriarty, N. W.; Holton, J. M.; Dobbek, H.; Brewster, A. S.; Adams, P. D.; Sauter, N. K.; Bergmann, U.; Zouni, A.; Messinger, J.; Kern, J.; Yachandra, V. K.; Yano, J. Untangling the sequence of events during the $S_2 \rightarrow S_3$ transition in photosystem II and implications for the water oxidation mechanism. *Proc. Natl. Acad. Sci. U. S. A.* **2020**, *117*, 12624−12635.
(15) de Paula, J. C.; Innes, J. B.; Brudvig, G. W. Electron transfer in photosystem II at cryogenic temperatures. *Biochemistry* **1985**, *24*, 8114−8120.
(16) Polander, B. C.; Barry, B. A. Detection of an intermediary, protonated water cluster in photosynthetic oxygen evolution. *Proc. Natl. Acad. Sci. U. S. A.* **2013**, *110*, 10634−10639.
(17) Miller, A.-F.; Brudvig, G. W. A guide to electron paramagnetic resonance spectroscopy of Photosystem II membranes. *Biochim. Biophys. Acta, Bioenerg.* **1991**, *1056*, 1−18.
(18) Vinyard, D. J.; Brudvig, G. W. Insights into substrate binding to the oxygen-evolving complex of photosystem II from ammonia inhibition studies. *Biochemistry* **2015**, *54*, 622−628.
(19) Peloquin, J. M.; Britt, R. D. EPR/ENDOR characterization of the physical and electronic structure of the OEC Mn cluster. *Biochim. Biophys. Acta, Bioenerg.* **2001**, *1503*, 96−111.
(20) Stich, T. A.; Yeagle, G. J.; Service, R. J.; Debus, R. J.; Britt, R. D. Ligation of D1-His332 and D1-Asp170 to the manganese cluster of photosystem II from *Synechocystis* assessed by multifrequency pulse EPR spectroscopy. *Biochemistry* **2011**, *50*, 7390−7404.
(21) Yeagle, G. J.; Gilchrist, M. L.; McCarrick, R. M.; Britt, R. D. Multifrequency pulsed electron paramagnetic resonance study of the S_2 state of the photosystem II manganese cluster. *Inorg. Chem.* **2008**, *47*, 1803−1814.
(22) Milikisiyants, S.; Chatterjee, R.; Weyers, A.; Meenaghan, A.; Coates, C.; Lakshmi, K. V. Ligand environment of the S_2 state of photosystem II: A study of the hyperfine interactions of the tetranuclear manganese cluster by 2D ^{14}N HYSCORE spectroscopy. *J. Phys. Chem. B* **2010**, *114*, 10905−10911.
(23) Milikisiyants, S.; Chatterjee, R.; Coates, C. S.; Koua, F. H. M.; Shen, J.-R.; Lakshmi, K. V. The structure and activation of substrate water molecules in the S_2 state of photosystem II studied by hyperfine sublevel correlation spectroscopy. *Energy Environ. Sci.* **2012**, *5*, 7747−7756.
(24) Rapatskiy, L.; Cox, N.; Savitsky, A.; Ames, W. M.; Sander, J.; Nowaczyk, M. M.; Rögner, M.; Boussac, A.; Neese, F.; Messinger, J.; Lubitz, W. Detection of the water-binding sites of the oxygen-evolving complex of photosystem II using W-band ^{17}O electron−electron double resonance-detected NMR spectroscopy. *J. Am. Chem. Soc.* **2012**, *134*, 16619−16634.
(25) Boussac, A.; Rutherford, A. W.; Sugiura, M. Electron Transfer Pathways from the S_2-states to the S_3-states either after a Ca^{2+}/Sr^{2+} or a Cl^-/I^- Exchange in Photosystem II from *Thermosynechococcus Elongatus*. *Biochim. Biophys. Acta, Bioenerg.* **2015**, *1847*, 576−586.

https://doi.org/10.1021/jacs.1c00633
J. Am. Chem. Soc. 2021, 143, 8324−8332

(26) Haumann, M.; Müller, C.; Liebisch, P.; Iuzzolino, L.; Dittmer, J.; Grabolle, M.; Neisius, T.; Meyer-Klaucke, W.; Dau, H. Structural and oxidation state changes of the photosystem II manganese complex in four transitions of the water oxidation cycle ($S_0 \rightarrow S_1$, $S_1 \rightarrow S_2$, $S_2 \rightarrow S_3$, and $S_{3,4} \rightarrow S_0$) characterized by X-ray absorption spectroscopy at 20 K and room temperature. *Biochemistry* **2005**, *44*, 1894−1908.
(27) Yano, J.; Pushkar, Y.; Glatzel, P.; Lewis, A.; Sauer, K.; Messinger, J.; Bergmann, U.; Yachandra, V. High-resolution Mn EXAFS of the oxygen-evolving complex in photosystem II: Structural implications for the Mn4Ca Cluster. *J. Am. Chem. Soc.* **2005**, *127*, 14974−14975.
(28) Cinco, R. M.; McFarlane Holman, K. L.; Robblee, J. H.; Yano, J.; Pizarro, S. A.; Bellacchio, E.; Sauer, K.; Yachandra, V. K. Calcium EXAFS establishes the Mn-Ca cluster in the oxygen-evolving complex of photosystem II. *Biochemistry* **2002**, *41*, 12928−12933.
(29) Iizasa, M.; Suzuki, H.; Noguchi, T. Orientations of carboxylate groups coupled to the Mn cluster in the photosynthetic oxygen-evolving center as studied by polarized ATR-FTIR spectroscopy. *Biochemistry* **2010**, *49*, 3074−3082.
(30) Guo, Z.; Barry, B. A. Cryogenic trapping and isotope editing identify a protonated water cluster as an intermediate in the photosynthetic oxygen-evolving reaction. *J. Phys. Chem. B* **2016**, *120*, 8794−8808.
(31) Debus, R. J. Evidence from FTIR Difference Spectroscopy That D1-Asp61 Influences the Water Reactions of the Oxygen-Evolving Mn4CaO5 Cluster of Photosystem II. *Biochemistry* **2014**, *53*, 2941−2955.
(32) Nakamura, S.; Noguchi, T. Infrared determination of the protonation state of a key histidine residue in the photosynthetic water oxidizing center. *J. Am. Chem. Soc.* **2017**, *139*, 9364−9375.
(33) Chatterjee, R.; Han, G.; Kern, J.; Gul, S.; Fuller, F. D.; Garachtchenko, A.; Young, I. D.; Weng, T.-C.; Nordlund, D.; Alonso-Mori, R.; Bergmann, U.; Sokaras, D.; Hatakeyama, M.; Yachandra, V. K.; Yano, J. Structural changes correlated with magnetic spin state isomorphism in the S_2 state of the $Mn4CaO_5$ cluster in the oxygen-evolving complex of photosystem II. *Chem. Sci.* **2016**, *7*, 5236−5248.
(34) Askerka, M.; Vinyard, D. J.; Wang, J.; Brudvig, G. W.; Batista, V. S. Analysis of the radiation-damage-free X-ray structure of photosystem II in light of EXAFS and QM/MM data. *Biochemistry* **2015**, *54*, 1713−1716.
(35) Narzi, D.; Mattioli, G.; Bovi, D.; Guidoni, L. A spotlight on the compatibility between XFEL and ab Initio structures of the oxygen evolving complex in photosystem II. *Chem. - Eur. J.* **2017**, *23*, 6969−6973.
(36) Pantazis, D. A.; Ames, W.; Cox, N.; Lubitz, W.; Neese, F. Two interconvertible structures that explain the spectroscopic properties of the oxygen-evolving complex of photosystem II in the S_2 state. *Angew. Chem., Int. Ed.* **2012**, *51*, 9935−9940.
(37) Siegbahn, P. E. M. Water oxidation energy diagrams for photosystem II for different protonation states, and the effect of removing calcium. *Phys. Chem. Chem. Phys.* **2014**, *16*, 11893−11900.
(38) Askerka, M.; Wang, J.; Vinyard, D. J.; Brudvig, G. W.; Batista, V. S. S_3 state of the O_2-evolving complex of photosystem II: Insights from QM/MM, EXAFS, and femtosecond X-ray diffraction. *Biochemistry* **2016**, *55*, 981−984.
(39) Narzi, D.; Bovi, D.; Guidoni, L. Pathway for Mn-cluster oxidation by tyrosine-Z in the S_2 state of photosystem II. *Proc. Natl. Acad. Sci. U. S. A.* **2014**, *111*, 8723.
(40) Retegan, M.; Krewald, V.; Mamedov, F.; Neese, F.; Lubitz, W.; Cox, N.; Pantazis, D. A. A five-coordinate Mn(IV) intermediate in biological water oxidation: Spectroscopic signature and a pivot mechanism for water binding. *Chem. Sci.* **2016**, *7*, 72−84.
(41) Pokhrel, R.; Brudvig, G. W. Oxygen-evolving complex of photosystem II: Correlating structure with spectroscopy. *Phys. Chem. Chem. Phys.* **2014**, *16*, 11812−11821.
(42) Askerka, M.; Wang, J.; Brudvig, G. W.; Batista, V. S. Structural changes in the oxygen-evolving complex of photosystem II induced by the S_1 to S_2 transition: A combined XRD and QM/MM study. *Biochemistry* **2014**, *53*, 6860−6862.
(43) Brahmachari, U.; Gonthier, J. F.; Sherrill, C. D.; Barry, B. A. Chloride maintains a protonated internal water network in the photosynthetic oxygen evolving complex. *J. Phys. Chem. B* **2017**, *121*, 10327−10337.
(44) Kawashima, K.; Takaoka, T.; Kimura, H.; Saito, K.; Ishikita, H. O_2 evolution and recovery of the water-oxidizing enzyme. *Nat. Commun.* **2018**, *9*, 1247.
(45) Wang, L.; Fried, S. D.; Boxer, S. G.; Markland, T. E. Quantum delocalization of protons in the hydrogen-bond network of an enzyme active site. *Proc. Natl. Acad. Sci. U. S. A.* **2014**, *111*, 18454.
(46) Milikisiyants, S.; Chatterjee, R.; Lakshmi, K. V. Two-dimensional ^{1}H HYSCORE spectroscopy of dimanganese di-μ-oxo mimics of the oxygen-evolving complex of photosystem II. *J. Phys. Chem. B* **2011**, *115*, 12220−12229.
(47) Randall, D. W.; Gelasco, A.; Caudle, M. T.; Pecoraro, V. L.; Britt, R. D. ESE-ENDOR and ESEEM characterization of water and methanol ligation to a dinuclear Mn(III)Mn(IV) complex. *J. Am. Chem. Soc.* **1997**, *119*, 4481−4491.
(48) Coates, C. S.; Milikisiyants, S.; Chatterjee, R.; Whittaker, M. M.; Whittaker, J. W.; Lakshmi, K. V. Two-dimensional HYSCORE spectroscopy of superoxidized manganese catalase: A model for the oxygen-evolving complex of photosystem II. *J. Phys. Chem. B* **2015**, *119*, 4905−4916.
(49) Beal, N. J.; Corry, T. A.; O'Malley, P. J. Comparison between experimental and broken symmetry density functional theory (BS-DFT) calculated electron paramagnetic resonance (EPR) parameters of the S_2 State of the oxygen-evolving complex of photosystem II in its native (calcium) and strontium-substituted form. *J. Phys. Chem. B* **2017**, *121*, 11273−11283.
(50) Zhang, C. Low-barrier hydrogen bond plays key role in active photosystem II — A new model for photosynthetic water oxidation. *Biochim. Biophys. Acta, Bioenerg.* **2007**, *1767*, 493−499.
(51) Saito, K.; Shen, J.-R.; Ishida, T.; Ishikita, H. Short hydrogen bond between redox-active tyrosine Y_Z and D1-His190 in the photosystem II crystal structure. *Biochemistry* **2011**, *50*, 9836−9844.
(52) Zaharieva, I.; Dau, H.; Haumann, M. Sequential and coupled proton and electron transfer events in the $S_2 \rightarrow S_3$ transition of photosynthetic water oxidation revealed by time-resolved X-ray absorption spectroscopy. *Biochemistry* **2016**, *55*, 6996−7004.
(53) Takemoto, H.; Sugiura, M.; Noguchi, T. Proton release process during the S_2-to-S_3 transition of photosynthetic water oxidation as revealed by the pH dependence of kinetics monitored by time-resolved infrared spectroscopy. *Biochemistry* **2019**, *58*, 4276−4283.
(54) Ishikita, H.; Saenger, W.; Loll, B.; Biesiadka, J.; Knapp, E.-W. Energetics of a possible proton exit pathway for water oxidation in photosystem II. *Biochemistry* **2006**, *45*, 2063−2071.
(55) Siegbahn, P. E. M. Water oxidation mechanism in photosystem II, including oxidations, proton release pathways, O——O bond formation and O_2 release. *Biochim. Biophys. Acta, Bioenerg.* **2013**, *1827*, 1003−1019.
(56) Kaur, D.; Szejgis, W.; Mao, J.; Amin, M.; Reiss, K. M.; Askerka, M.; Cai, X.; Khaniya, U.; Zhang, Y.; Brudvig, G. W.; Batista, V. S.; Gunner, M. R. Relative stability of the S_2 isomers of the oxygen evolving complex of photosystem II. *Photosynth. Res.* **2019**, *141*, 331−341.
(57) Vinyard, D. J.; Khan, S.; Askerka, M.; Batista, V. S.; Brudvig, G. W. Energetics of the S_2 state spin isomers of the oxygen-evolving complex of photosystem II. *J. Phys. Chem. B* **2017**, *121*, 1020−1025.
(58) Boussac, A. Temperature dependence of the high-spin S_2 to S_3 transition in Photosystem II: Mechanistic consequences. *Biochim. Biophys. Acta, Bioenerg.* **2019**, *1860*, 508−518.
(59) Boussac, A.; Ugur, I.; Marion, A.; Sugiura, M.; Kaila, V. R. I.; Rutherford, A. W. The low spin - high spin equilibrium in the S_2-state of the water oxidizing enzyme. *Biochim. Biophys. Acta, Bioenerg.* **2018**, *1859*, 342−356.
(60) Vinyard, D. J.; Khan, S.; Brudvig, G. W. Photosynthetic water oxidation: binding and activation of substrate waters for O−O bond formation. *Faraday Discuss.* **2015**, *185*, 37−50.

https://doi.org/10.1021/jacs.1c00633
J. Am. Chem. Soc. 2021, 143, 8324−8332

(61) Drosou, M.; Zahariou, G.; Pantazis, D. A. Orientational Jahn–Teller isomerism in the dark-stable state of nature's water oxidase. *Angew. Chem., Int. Ed.* **2021**, DOI: 10.1002/anie.202103425.
(62) Zahariou, G.; Ioannidis, N.; Sanakis, Y.; Pantazis, D. A. Arrested substrate binding resolves catalytic intermediates in higher-plant water oxidation. *Angew. Chem., Int. Ed.* **2021**, *60*, 3156–3162.

https://doi.org/10.1021/jacs.1c00633
J. Am. Chem. Soc. 2021, 143, 8324–8332